Current Photovoltaic Research 9(3) 96-105 (2021)
DOI:https://doi.org/10.21218/CPR.2021.9.3.096
pISSN 2288-3274
eISSN 2508-125X

Characterization of an In_2Se_3 Passivation Layer for CIGS Solar Cells with Cd-free Zn-containing Atomic-layer-deposited Buffers

Suncheul Kim[1,2] · Ho Jin Lee[1] · Byung Tae Ahn[1]* · Dong Hyeop Shin[3] · Kihwan Kim[3] · Jae Ho Yun[3]*

[1]Department of Material Science and Engineering, Korea Advanced Institute of Science and Technology, Daejeon 34141, Korea
[2]Metal Process Technology Team, Memory Division, Samsung Electronics, Gyunggi 18448, Korea
[3]Photovoltaic Team, Korea Institute of Energy Research, Daejeon 34129, Korea

Received July 26, 2021; Revised September 6, 2021; Accepted September 9, 2021

ABSTRACT: Even though above 22% efficiencies have been reported in Cd-free $Cu(In,Ga)Se_2$ (CIGS) solar cell with Zn-containing buffers, the efficiencies with Zn-containing buffers, in general, are well below 20%. One of the reasons is Zn diffusion from the Zn-containing buffer layer to CIGS film during buffer growth. To avoid the degradation, it is necessary to prevent the diffusion of Zn atoms from Zn-containing buffer to CIGS film. For the purpose, we characterized an In_2Se_3 film as a possible diffusion barrier layer because In_2Se_3 has no Zn component. It was found that an In_2Se_3 layer grown at 300°C was very effective in preventing Zn diffusion from a Zn-containing buffer. Also, the In_2Se_3 had a large potential barrier in the valence band at the In_2Se_3/CIGS interface. Therefore, In_2Se_3 passivation has the potential to achieve a super-high efficiency in CIGS solar cells that employ Cd-free ALD processed buffers containing Zn.

Key words: $Cu(In,Ga)Se_2$ solar cells, In_2Se_3 passivation layer, Zn diffusion, hole blocking

1. Introduction

Recently, an efficiency of 23.35% was reported in CIGS solar cells by employing Zn(O,S,OH)/ZnMgO double-layer buffer[1], and 22% efficiency was reported by employing $Zn_{0.8}Mg_{0.2}O$ buffer and $Zn_{0.9}Mg_{0.1}O$:B transparent conductive oxide layers[2, 3]. However, such results are still lower than the record efficiencies in Si and GaAs solar cells. The main cause of lower efficiency in CIGS solar cells is a low voltage gain ratio (~0.65) compared to those of Si and GaAs solar cells (~0.8), where the voltage gain ration is defined as qV_{oc}/Eg, where q, V_{oc}, and E_g are proton charge, open-circuit voltage, and band gap, respectively. In this respect, reducing the surface recombination rate in CIGS solar cells is one of the key factors to increase the voltage gain ratio.

In the CIGS solar cell, buffer layers including CdS, Zn(S,O,OH), ZnMgO, and ZnSnO have been introduced to increase the cell performance, especially, V_{oc}. The CdS and Zn(S,O,OH) buffers were deposited by the chemical bath deposition (CBD) method. However, the CBD method is inappropriate for mass production due to uniformity issues, chemical waste treatment issues, and reproducibility problems. In this regard, the atomic layer deposition (ALD) process of buffers including ZnSO, ZnMgO, and ZnSnO is favorable because the ALD process could provide better uniformity in larger areas, better control of thickness, and less chemical waste. Somehow, most Cd-free buffers prepared by the ALD process have consisted of a Zn component in buffers. More details on Cd-free buffers and ALD process can be seen in a recent review paper[4].

In general, compared to CIGS solar cells with CBD CdS buffer, CIGS solar cells with Zn-containing ALD buffers including ZnSO, ZnMgO, and ZnSnO buffers had lower open circuit voltage (V_{oc})[4-6]. During the ALD process, the CIGS substrate was heated for the ALD process to around 120°C, where Zn atoms diffuse into CIGS film through the copper vacancy sites[7-9].

Fig. 1 shows the Zn depth profile in CIGS film after ALD ZnMgO growth at 120°C, which caused the V_{oc} and FF of the CIGS solar cells to degrade in our previous report[10]. For this reason, the Zn diffusion into CIGS film should be prevented by introducing a diffusion barrier material in which Zn component is not included.

In the present paper, to prevent the Zn diffusion from ALD Zn-containing buffer to CIGS, we introduce an In_2Se_3 layer as a diffusion barrier on the CIGS surface. The main purpose was to

*Corresponding author: btahn@kaist.ac.kr; yunjh92@kier.re.kr

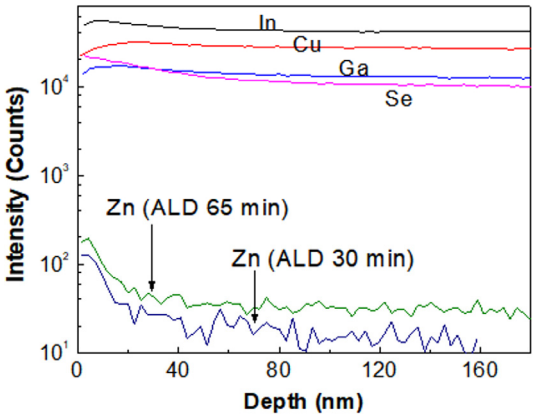

Fig. 1. Zn diffusion into CIGS film during ALD ZnSnO buffer growth at 120°C for two-different growing times[10)]

prevent Zn diffusion from the Zn-containing ALD buffer during the ALD process because In_2Se_3 does not contain Zn atoms and can absorb Zn from Zn-containing buffers.

The second purpose was to reduce the interface recombination rate at the CIGS surface. The In_2Se_3 layer with a wide band gap can serve as a hole-blocking layer, like the commonly-used buffer layers in most CIGS solar cells. Commonly-used buffers employed in CIGS solar cells are either sulfides or oxides or oxygen-containing sulfides. The ionic radii of oxygen (0.132 nm) and sulfide (0.174 nm) are smaller than that of selenium (0.191 nm) so that interface between the commonly-used buffer and CIGS absorber can have many defects due to lattice mismatch, causing a high surface recombination rate. The examples of good lattices at the CIGS surface include a $K(In,Ga)Se_2$ layer by NaF+KF PDT[11, 12)] and a $Cu(In,Ga)_3Se_5$ layer by Se PDT[13)]. These layers, consisting of Se as the main matrix component, are a hole-blocking layer and epitaxy layer on CIGS film. However, a sturdier hole-blocking layer than those $K(In,Ga)Se_2$ or $Cu(In,Ga)Se_2$ layers is needed to achieve a higher voltage gain in CIGS solar cells. The band gap of In_2Se_3 is above 2 eV[14, 15)] and can have a hole-blocking barrier in contact with CIGS. Both In_2Se_3 and CIGS could have less interface defects because the matrix ions of both phases are Se ions, resulting in better lattice match than oxide- and sulfide-containing buffers. For example, $CuIn_3Se_5$ and $CuInSe_2$ have the Se-based crystal matrix Therefore, $CuIn_3Se_5$ phase on $CuInSe_2$ phase can have a partial epitaxial interface[16)]. It was found that a better epitaxial interface was grown from the evaporation of molecular sources such as In_2Se_3 and Cu_2Se[16)].

In adapting In_2Se_3 as a Zn diffusion barrier, one more restriction should be considered. Out-diffusion of copper from CIGS absorber to In_2Se_3 thin layer should be blocked to avoid forming $CuInSe_2$ phase. The Cu concentration at the CIGS surface is high in the as-deposited CIGS film and low in the CIGS surface by Se PDT or NaF PDT[13, 17, 18)]. Pure In_2Se_3 was successful grown at 300°C, and Zn diffusion into CIGS film was prevented by a 20-nm-thick In_2Se_3 layer. The details of In_2Se_3 growth on CIGS film, barrier characteristics on Zn diffusion, and a potential hole-blocking barrier are described in the Results and Discussion section.

2. Experimental

First, In_2Se_3 film was deposited by co-evaporation of In and Se elements on a glass or Mo substrate at 300°C to characterize the optical properties of In_2Se_3 film. The fluxes of indium and selenium were 0.8 and 1.5 nm/s, respectively. The deposition rate of In_2Se_3 thin layer was about 0.6 nm/s. For passivation purposes, In_2Se_3 thin layers with various thicknesses were deposited on the CIGS film by the same co-evaporation process on 1.8-μm-thick CIGS film that was also deposited by a three-stage co-evaporation process at 550°C[13, 17)]. Then, 40-nm-thick $Zn_{0.8}Sn_{0.1}O$ was deposited by ALD process at 120°C for 30 min, at which Zn could diffuse into CIGS through the In_2Se_3 passivation film[19)]. The $Zn_{0.8}Sn_{0.2}O$ composition was prepared by a 4:1 cycle ratio of ZnO ALD process (DEZ 0.1 s, purge 2 s, H_2O 0.1 s, purge 3 s) and SnO_2 ALD process (TDMA-Sn 0.1 s, purge 2 s, H_2O 0.1 s, purge 3 s). With this experiment, we reported a 17.22% cell efficiency in the ZnSnO/CIGS structure without alkali post deposition treatment and AR coating[19)].

The microscopic image and composition of the films were examined by field-emission scanning electron microscope (SEM), transmission electron microscope (TEM), and electron dispersive spectroscopy (EDS) using FEI Nova23 with resolutions of 1.0 and 1.6 nm at 15 kV and 1 kV, respectively. The transmittance spectrum and reflectance spectrum were measured using a JASCO V-650 spectrophotometer at wavelengths ranging from 190 to 900 nm with an accuracy of 0.2 nm. The low-temperature photoluminescence (LTPL) spectra were measured at 10 K using LabRAM HR UV/Vis/NIR PL made by Horiba Jobin Yvon with a 514-nm laser. The wavelength of the laser source was 514 nm, and the power of the laser was controlled by filters. The x-ray photoelectron spectroscopy (XPS) of the Cu 2p3/2 spectra and valance band were measured using K-alpha made by Thermo VG Scientific. The Raman spectra of the films were measured using LabRAM HR Evolution Visible-NIR made by HORIBA. The depth profiles of elements in the films were

measured by secondary ion microscopy (SIMS) with TOF-SIMS5 made by ION-TOF GmbH. Before depth profiling, the 40-nm-thick ZnSnO buffer on the films was etched by hydrochloric acid solution for about ten seconds to avoid a knock-on effect in CIGS film. With the chemical etching, only oxide was removed and selenide was not etched[20].

3. Results and Discussion

3.1 Optical characterization of In_2Se_3 thin film

To adopt In_2Se_3 as a passivation layer, the optical properties of In_2Se_3 were investigated first. Fig. 2 shows an SEM image (a) and EDS result (b) of a 300-nm-thick In_2Se_3 film deposited at 300°C on a Mo substrate.

The SEM and EDS results were taken at 20 k and 10 k magnifications, respectively. The SEM image showed a flat surface without any pinhole or bump. From the EDS result, the compositions of In and Se were 41.6% and 58.4, respectively, and the film was slightly Se poor compared to the ideal case of In_2Se_3 (40% In and 60%Se). The Raman spectroscopy of the In_2Se_3 layer, not shown here, was well matched to the Raman spectroscopy data of γ-In_2Se_3 reported in literature[21, 22].

Fig. 3 shows the optical transmittance and reflectance (a) and Tauc plot (b) of a 300-nm-thick In_2Se_3 film deposited at 300°C on a glass substrate. The transmittance of In_2Se_3 became monotonically lowered from 0.8 to 0.1 as the wavelength decreased from 800 to 600 nm. The reflectance of In_2Se_3 reached a maximum broad peak at 700 nm wavelength and minimum peaks at 600 and 820 nm due to thickness interference.

With the transmittance and reflectance data, the absorption coefficient was obtained. Then the band gap of In_2Se_3 was determined by absorption coefficient and Tauc plot in Fig. 3(b). The band gap of In_2Se_3 was measured to be 1.93 eV.

Fig. 4 showed the LTPL spectra of 300-nm-thick In_2Se_3 film deposited on Mo substrate, with various power densities for a 514-nm laser at 10 K. In the low excitation powers from 0.1 to 1 mW, two peaks (P1 at 2.13 eV and P2 at 2.11 eV) were observed. At 2.5 mW power, an additional weak peak with a low

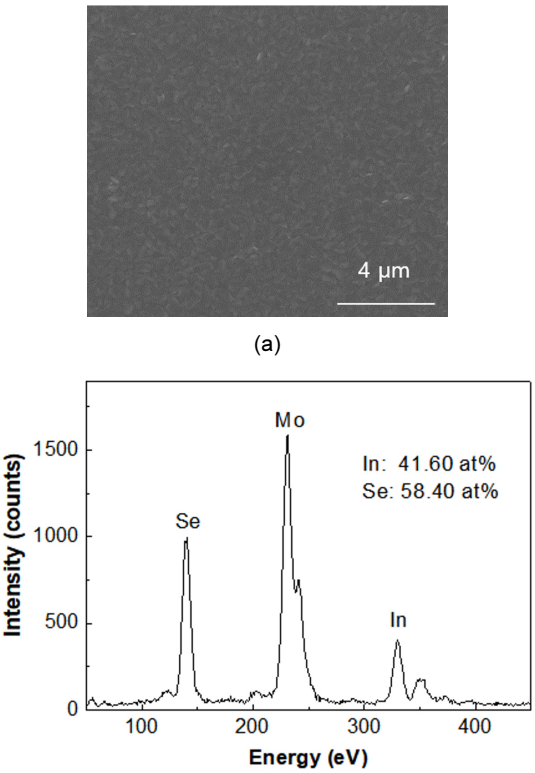

Fig. 2. SEM surface image (a) and EDS intensity of 300-nm thick In_2Se_3 film deposited on glass substrate by co-evaporation of In and Se at 300°C

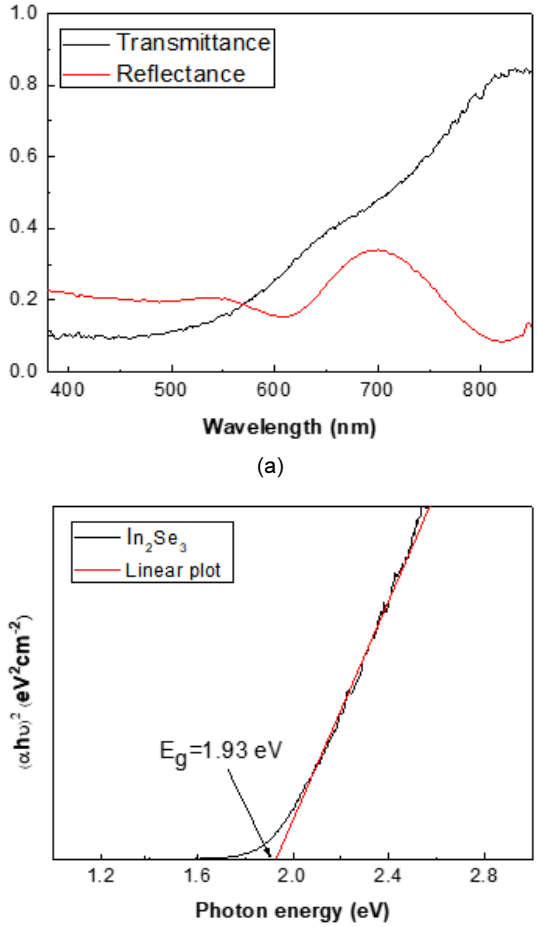

Fig. 3. Optical measurement of 300-nm thick In_2Se_3 film deposited on glass substrate by co-evaporation of In and Se at 300°C

emission energy was observed at 2.05 eV. The peak intensity versus excitation power density can be given as

$$I_{PL} \propto p_{exc}^{k} \quad (1)$$

where p_{exc} is the excitation power, I_{PL} is the PL intensity at a specific excitation power, and k is the characteristic parameter for the emission peak.

The change of P1 peak intensity as a function of excitation power is shown in Fig. 5. From the log-log fitting of the data, the value of k was 1.3. The exciton is considered as a band-to-band transition for k > 1, and the exciton was considered as a free-to-bound transition or a donor-to-acceptor pair recombination for k < 1[23-25]. This means that the P1 peak corresponds to band-to-band transition. The difference of photon energy between P1 and P2 is about 17 meV at 10 K.

The ionization energy of selenium was about 40 meV, and the electron affinity of indium was about 38 meV. In addition, T. Ohtsuka et al. mentioned that the activation energy for bound exciton emissions of In_2Se_3 was greater than 22 meV[26]. Therefore, the P2 peak is expected to be a phonon replica of the P1 peak.

The P3 peak was located about 62 meV below the P2 peak or 79 meV below the P1 peak. Since the stoichiometry of the In_2Se_3 film deposited at 300°C in our experiment was Se poor, it was believed that the peak originated from the selenium vacancy with a very low concentration. The PL analysis signifies that the quality of In_2Se_3 film itself was good and the recombination In_2Se_3 film could be negligible.

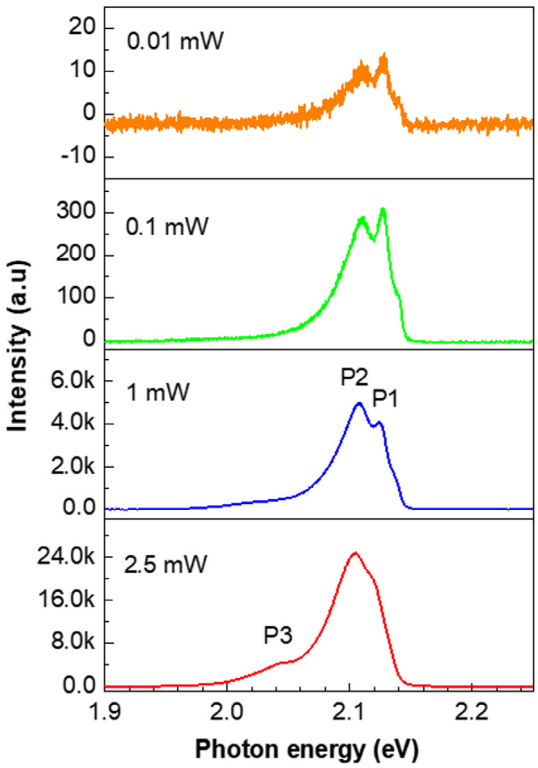

Fig. 4. LTPL spectra of In_2Se_3 film at 10K with various laser power densities with 514-nm wavelength

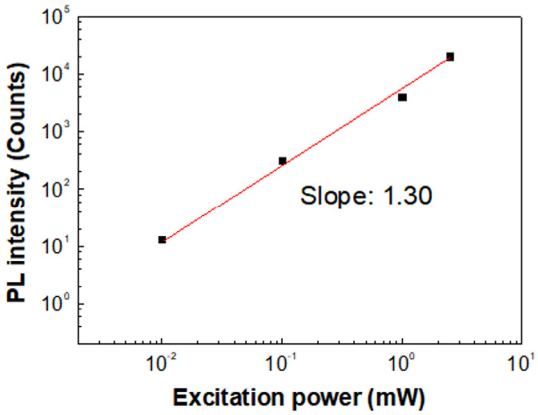

Fig. 5. LTPL intensity change of P1 peak in the In_2Se_3 film as a function of excitation power

3.2 Growth of In_2Se_3 on CIGS film

Unlike depositing an In_2Se_3 layer on glass or molybdenum substrate, upon growing an In_2Se_3 layer on CIGS film, there is a reaction between In_2Se_3 and the CIGS substrate due to the rapid out-diffusion of copper atoms from the CIGS substrate. The Cu diffusion into In_2Se_3 can form a $CuInSe_2$ phase that has a lower band gap than CIGS, causing degradation of device performance.

Fig. 6 shows the XPS depth profiles of Cu/(In+Ga) ratios in the as-deposited CIGS film prepared at 550°C by co-evaporation process and in the CIGS with NaF post-deposition-treatment (PDT) at 300°C[17]. This figure was taken to explain the Zn diffusion mechanism during the In_2Se_3 deposition. The Cu/(In+Ga)

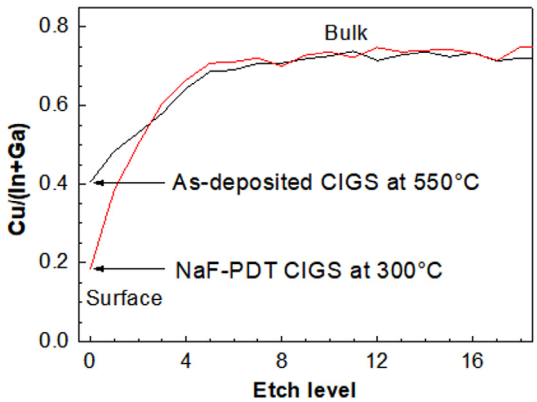

Fig. 6. AES depth profiles of Cu/(In+Ga) ratio in the as-deposited CIGS film at 550°C and NaF-PDT CIGS film at 300°C[17]

ratio on the surface of the as-deposited CIGS was 0.4, while that on the CIGS surface with NaF PDT was less than 0.2. With the NaF PDT process, the Cu/(In+Ga) ratio lowered substantially because Na alkali atoms occupy Cu sites and because Cu atoms were pushed away from the surface. Therefore, in case of CIGS film with alkali PDT, the out-diffusion of Cu from CIGS to In_2Se_3 film during In_2Se_3 growth could be greatly suppressed.

To investigate a worst-case scenario or for possible elimination of the PDT process, an In_2Se_3 layer was grown on the as-deposited CIGS film at two different temperatures (300 and 400°C) by co-evaporating. Fig. 7 shows the Raman spectra of In-Se layers grown at 300°C and 400°C by supplying In and Se on as-deposited CIGS film and an in-Se layer grown at 300°C on a Mo substrate. The term In-Se layer means the layer grown by the ALD process but the phase is not defined correctly yet. The peaks of the In_2Se_3 phase and CIGS phase are located at 150 and 175 /cm, respectively, in Raman spectroscopy[27, 28].

To detect photoelectron emission near the surface region, laser intensity was minimized by a laser filter just before the major peaks of CIGS and In_2Se_3. On the Mo substrate, a sharp In_2Se_3 peak was observed, indicating that an In_2Se_3 phase with a good crystallinity can be grown at 300°C. For the growth at 400°C on the CIGS substrate, only a $CuInSe_2$ peak was observed, and no In_2Se_3 peak was observed, indicating that 400°C was too high of a temperature to grow an In_2Se_3 layer on a CIGS substrate. At 300°C growth on a CIGS substrate, both In_2Se_3 and CIGS peaks were observed.

Fig. 8 shows TEM cross-sectional images of the In-Se layers grown at (a) 300°C and (b) 400°C on the as-deposited CIGS film that was prepared at 550°C. The film grown at 300°C for 30 min was around 50 nm. Since the thickness of In_2Se_3 grown at 300°C was very thin, the peak from the CIGS substrate was also observed. The film grown at 400°C for 30 min was $CuInSe_2$ phase with more than 300-nm thickness, which was validated by Raman spectroscopy.

To further confirm the compositions in those layers, EDS composition analysis was conducted both In_2Se_3/CIGS interface

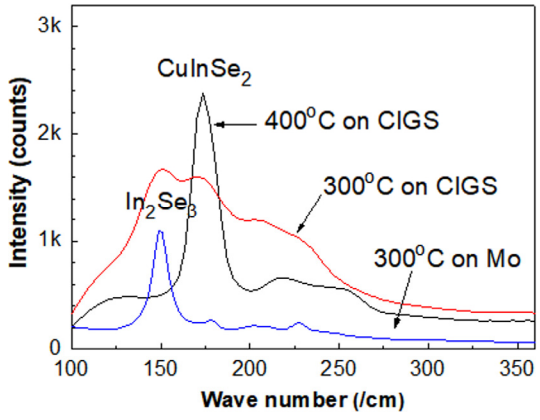

Fig. 7. Raman spectra of In-Se layers grown at 300°C and 400°C by supplying In and Se on as-deposited CIGS film and an in-Se layer grown at 300°C on Mo substrate

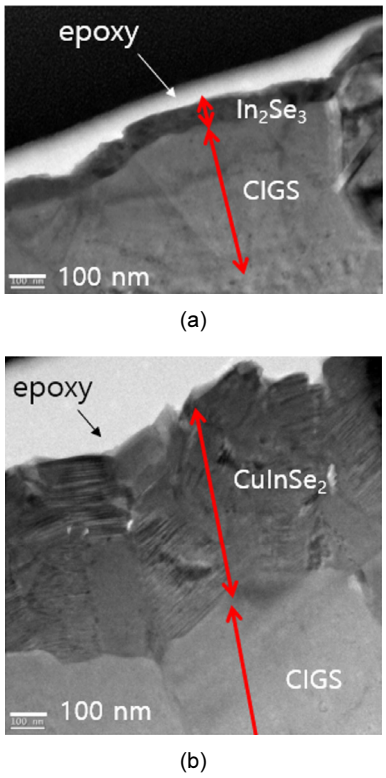

Fig. 8. TEM cross-sectional images of In-Se layers grown at 300°C (a) and 400° (b), by supplying In and Se on as-deposited CIGS film which was grown at 550°C

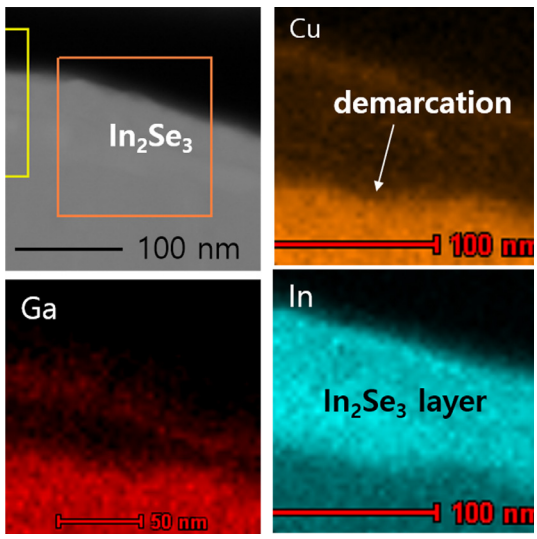

Fig. 9. Cross-sectional EDS analysis of In_2Se_3/CIGS film, where the In_2Se_3 layer was grown at 300°C by supplying In and Se on as-deposited CIGS film

and $CuInSe_2$/CIGS interface. Fig. 9 shows the cross-sectional EDS analysis of the In_2Se_3/CIGS film, where the In_2Se_3 layer was grown at 300°C by supplying In and Se on as-deposited CIGS film. In the In_2Se_3 region, the Ga and Cu intensities were negligible, while the In intensity was very high. From the Cu, Ga, and In distribution, the demarcation between In_2Se_3 and CIGS was clearly shown. Therefore, it was considered that the 50-nm-thick layer on the CIGS surface was In_2Se_3 phase. The EDS image could not exclude the existence of Cui and Ga as solid solution.

Fig. 10 shows the cross-sectional EDS analysis of $CuInSe_2$/CIGS film, where the $CuInSe_2$ layer was grown at 400°C by supplying In and Se on CIGS film. The images shown in Fig. 10 cover $CuInSe_2$ phase with a thick layer (>300 nm). In the $CuInSe_2$ region, the Ga intensity was negligible, while both the Cu and In intensities were very high. This indicates that Cu atoms were diffused out and Ga atoms were not diffused out from the CIGS surface at 400°C process.

Fig. 11 shows the XPS depth spectra of Cu 2p3/2 on the In_2Se_3 surface layer (a) and on the $CuInSe_2$ surface layer (b). The In_2Se_3 and $CuInSe_2$ layers were grown at 300°C and 400°C, respectively, by supplying In and Se on the as-deposited CIGS film.

In the case of 300°C growth, a copper peak was not detected in the In_2Se_3 layer for 1st and 2nd etch levels and barely detected at the 3rd etch level. From EDS analysis the existence of Cu and Ga was not negligible. But, From the XPS analysis it was seen that Cu was excluded from the top surface. This confirms that a pure In_2Se_3 formed at 300°C growth at the CIGS surface up to 2nd level. Since the resolution of XPS is around 1%, pure In_2Se_3 means the Cu content is below 1%.

The Cu detected in the fourth etch level could be the originated from the substrate CIGS film. The demarcation between In_2Se_3 and CIGS was not clear in the XPS depth profile due to interface roughness. In the case of 400°C growth, copper was detected from the surface of $CuInSe_2$ layer and throughout the $CuInSe_2$ film, confirming that $CuInSe_2$ surface layer exists.

From the Raman spectroscopy, TEM images, EDS analysis, and XPS analysis, it was confirmed that a pure In_2Se_3 layer could be grown at 300°C on as-deposited CIGS film. Since the Cu/(In+Ga) ratio on the surface of CIGS film with an alkali PDT process is about one-half of the ratio on the as-deposited CIGS film, growing a pure In_2Se_3 layer at 300°C is much more likely.

3.3 Zinc suppression in CIGS interface with an In_2Se_3 layer

As we mentioned in the Introduction section, in CIGS, zinc atoms can easily move from buffer layer to CIGS through copper vacancies sites in the CIGS film because the CIGS film used for solar cell application has a Cu-poor stoichiometry. To determine the diffusion length of zinc in In_2Se_3 and CIGS films,

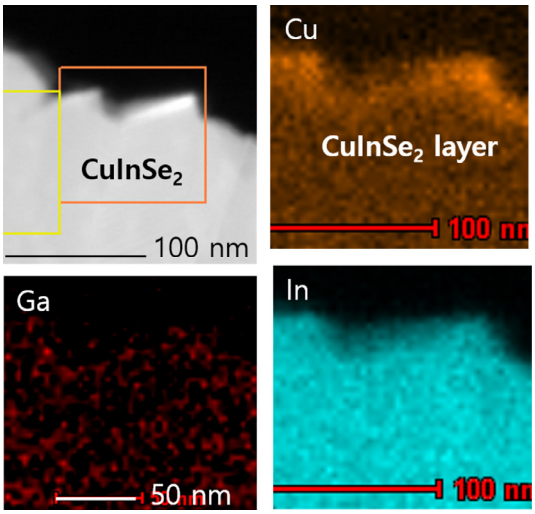

Fig. 10. Cross-sectional EDS analysis of $CuInSe_2$/CIGS film, where In_2Se_3 layer was grown at 400°C by supplying In and Se on CIGS film

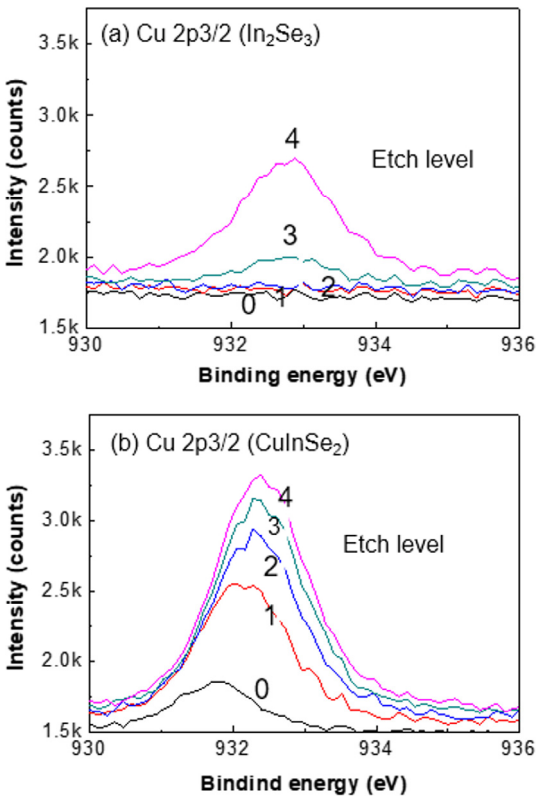

Fig. 11. XPS depth spectra of Cu with the In_2Se_3 surface layer (a) and with the $CuInSe_2$ surface layer (b)

a ZnSnO buffer layer was deposited on an In_2Se_3 film and on a CIGS film by the ALD process, which was described in the experimental section. The 300-nm thick In_2Se_3 film was grown at 300°C on the as-deposited CIGS film.

Fig. 12 shows the SIMS depth profiles of zinc atoms on the surfaces of the as-deposited CIGS film, NaF-PDT CIGS film, and In_2Se_3 film. The as-deposited CIGS film was prepared at 550°C, and the NaF PDT process was conducted at 300°C[19]. A ZnSnO buffer layer was deposited on these films at 300°C for 30 min by an ALD process and was etched off with an HCl solution to avoid the knock-on effect during the SIMS depth profile. With the chemical etching, only oxide was removed and selenide was not etched[20].

On the as-deposited CIGS film, the Zn concentration at the CIGS surface was high, and zinc atoms penetrated above 100 nm from the CIGS surface. On the NaF-PDT CIGS film, the intensity of Zn at the surface was one order of magnitude lower than that on the as-deposited CIGS film. The reason of low Zn intensity at the surface with NaF PDT is due to no available Cu vacancy sites by Na occupation by NaF PDT. Zn atoms can easily diffuse through interstitial sites. However, the Zn intensity in the 50- to 120-nm depth was similar to that of as-deposited CIGS film. This indicates that the Zn concentration at the CIGS surface can be greatly reduced at the surface but that, in the subsurface, the Zn concentration is not negligible. On the In_2Se_3 film, the intensity of Zn at the surface was one order of magnitude lower than that of as-deposited CIGS film and similar to that of NaF-PDT CIGS film. It was noted that the Zn intensity was rapidly diminished in the case of depth less than 30 nm. In this case, the Zn intensity at 20-nm depth was one-tenth lower than that of the base intensity in CIGS film. This indicates clearly that In_2Se_3 film is a highly effective barrier material for Zn diffusion.

By using the data from Fig. 12 and the general solution for Fick's second law,

$$\frac{\partial c}{\partial t} = D\frac{\partial^2 y}{\partial x^2}, \quad C = A + B\, erf\left(\frac{x}{2\sqrt{Dt}}\right) \tag{2}$$

the relative values of diffusion coefficient were calculated. The zinc diffusion coefficient ratio, in as-deposited CIGS and in In_2Se_3, $D_{Zn}(CIGS)/D_{Zn}(In_2Se_3)$, was about 11. Again, our result showed that In_2Se_3 layer can have a major advantage as a Zn diffusion barrier for a CIGS absorber that adopts Cd-free ALD buffers containing Zn.

Fig. 13 shows the SIMS depth profile of Zn atoms in the as-deposited CIGS films with or without an In_2Se_3 passivation layer. An ALD ZnSnO buffer was deposited at 120°C for 30 min on these films and chemically etched off before depth analysis. 20-nm-thick and 50-nm-thick In_2Se_3 layer were deposited on the CIGS absorber layer to verify the thickness effect of the In_2Se_3 layer.

The SIMS intensity of Zn atoms was sharply diminished with the In_2Se_3 passivation layer, and the base intensity throughout the CIGS film in the In_2Se_3/CIGS structures was again one order of magnitude smaller. Therefore, the In_2Se_3 layers with both 20-nm and 50-nm thicknesses performed well as a diffusion barrier of zinc atoms from ALD ZnSnO buffer to CIGS absorber.

The depth profile of Zn atoms with a 20-nm-thick In_2Se_3 layer was similar as that of Zn atoms with 50-nm thickness in Fig. 13. A thinner In_2Se_3 film can have advantages with less series resistance, less light scattering, and short process time. Since controlling the thickness of In_2Se_3 below 20 nm was difficult in practice in our co-evaporation process, it seemed that

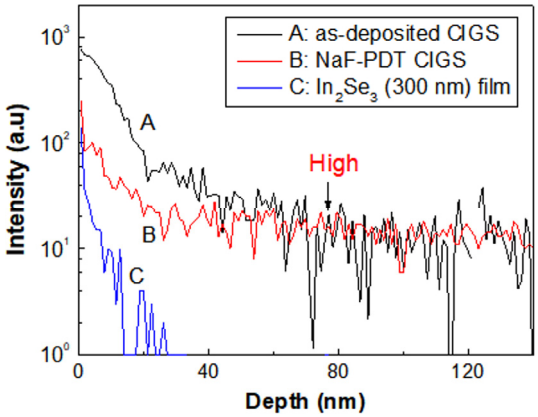

Fig. 12. SIMS depth profiles of Zn atoms on the surfaces of as-deposited CIGS film, NaF-PDT CIGS film, and In_2Se_3 film

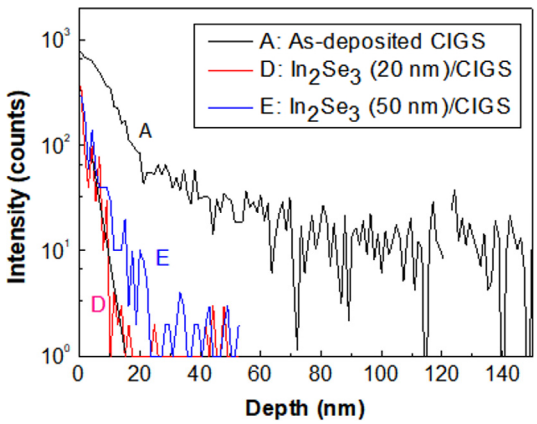

Fig. 13. SIMS depth profiles of Zn atoms in the as-deposited CIGS film with and without In_2Se_3 passivation layer

a 20-nm-thick In_2Se_3 layer was the optimum condition as a Zn diffusion barrier at the ALD ZnSnO/CIGS interface.

3.4 Band structure of In_2Se_3/CIGS film

Fig. 14 shows the XPS valance-band spectra at the surfaces of the as-deposited CIGS film prepared at 550°C, of the NaF-PDT CIGS film processed at 300°C, and of the In_2Se_3 film grown at 300°C on the as-deposited CIGS substrate. The valence band maximum (VBM) of each film can be determined by the extrapolation of maximum slope from the spectra. The VBM values of the as-deposited CIGS, NaF-PDT CIGS, and In_2Se_3 were -0.4. -0.52, and -1.2 eV, respectively, from the Fermi level.

Fig. 15 shows the electronic band structure of In_2Se_3/CIGS interface after the NaF-PDT process, constructed based on the XPS results and optical measurement. Valence band offset (VBO) is the VBM difference between two different regions or materials. The VBO value between the CIGS surface after NaF PDT and the CIGS surface of the as-deposited CIGS was 0.12 eV. The VBM lowering by NaF PDT, named as PDT layer, serves as a hole-blocking layer[17]. The VBO value between the In_2Se_3 layer and NaF-PDT CIGS surface was 0.68 eV, which was five times larger than 0.12 eV. Therefore, the In_2Se_3 layer can be a good candidate as for hole-blocking layer. Based on the excellent barrier for Zn diffusion during Zn-containing ALD buffer and good band alignment at the In_2Se_3/CIGS surface, it is expected that the insertion of an In_2Se_3 layer can be an excellent passivation layer for CIGS solar cells that consist of Cd-free ALD buffers containing Zn and can have serious potential to achieve super-high-efficiency Cd-free CIGS solar cells. Device fabrication with In_2Se_3 buffer is beyond the scope of this paper.

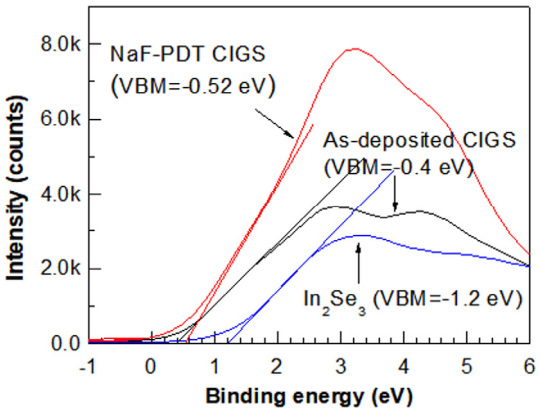

Fig. 14. XPS valance band spectra at the surfaces of as-deposited CIGS, NaF-PDT CIGS, and In_2Se_3 films

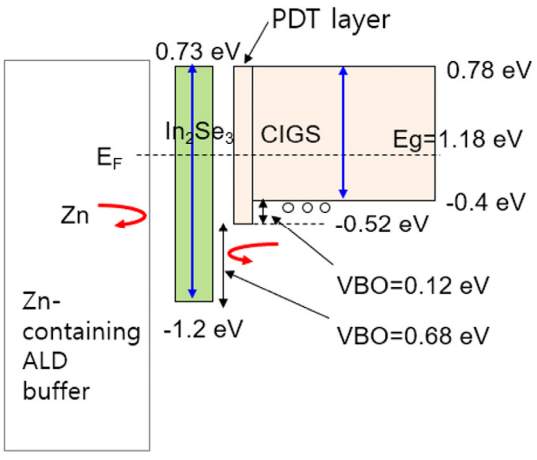

Fig. 15. Schematic of electronic band structure with In_2Se_3 passivation layer in Zn-containing buffer/NaF-PDT CIGS structure

4. Conclusions

Due to the Zn diffusion from Zn-containing ALD buffers into CIGS film during the ALD process of growing a buffer layer, the cell performance of the CIGS solar cell was degraded. To prevent Zn diffusion, an In_2Se_3 layer that has no Zn component was characterized as having potential use as a passivation layer at the Zn-containing ALD buffer/CIGS interface. The In_2Se_3 film grown at 300°C by co-evaporating In and Se elements showed a Se-poor stoichiometry with a band gap of 1.93 eV. A Se-vacancy-related defect was barely detected in the LTPL spectrum at a high excitation energy of 2.5 mW.

Growth of In_2Se_3 film on the CIGS substrate was greatly affected by the growth temperature. At 400°C, $CuInSe_2$ phase was grown instead of In_2Se_3 because Cu atoms were diffused out to the In_2Se_3 layer. At 300°C, a pure In_2Se_3 phase was grown, indicating that an In_2Se_3 layer should be grown at or below 300°C. Raman spectra, TEM images, EDS analysis, and XPS analysis confirmed that a thin In_2Se_3 with no Cu can be grown at 300°C on a CIGS substrate by co-evaporating In and Se.

With ALD ZnSnO process at 120°C for 30 min, the diffusion of Zn atoms into the In_2Se_3 layer was limited to about 20 nm, while that into CIGS film was more than 100 nm. Of note, the SIMS base intensity of Zn atoms in In_2Se_3 film was one order of magnitude lower than that in CIGS film, where Zn diffused rapidly through Cu-vacancy sites in the CIGS film. The 20-nm-thick In_2Se_3 layer in the ZnSnO/ In_2Se_3/CIGS structure demonstrated that Zn diffusion into CIGS film can be effectively prevented.

The VBO value between In_2Se_3 layer and the CIGS surface after NaF-PDT was 0.68 eV, while the value between the CIGS

surface after NaF PDT and the CIGS surface for as-deposited film was 0.12 eV. It suggests that the In_2Se_3 can serve as an effective hole-blocking layer.

Based on its excellent diffusion barrier of Zn atoms from Zn-containing ALD buffer and good band alignment with large VBO at the In_2Se_3/CIGS interface, it is expected that the insertion of an In_2Se_3 layer deposited at or just below 300°C can be an excellent passivation layer for CIGS solar cells and can lead to a super-high efficiency in Cd-free CIGS solar cells. Device fabrication with In_2Se_3 buffer is beyond the scope of this paper.

Acknowledgment

This work was financially supported by the Technology Development Program to Solve Climate Change of the National Research Foundation of Korea (No. 2016M1A2A2936757) and by the Korea Institute of Energy Technology Evaluation and Planning (No.20163030013690).

References

1. M. Nakamura, K. Yamaguchi, Y. Kimoto, Y. Yasaki, Cd-Free Cu(In,Ga)(Se,S)$_2$ thin-film solar cell with record efficiency of 23.35%, IEEE J. Photovoltaics, 9, 1863-1867 (2019).
2. J. Chantana, Y. Kawano, T. Nishimura, Y. Kimoto, T. Kato, H. Sugimoto, T. Minemoto, 22%-efficient Cd-free Cu(In,Ga)(S,Se)$_2$ solar cell by all-dry process using $Zn_{0.8}Mg_{0.2}O$ and $Zn_{0.9}Mg_{0.1}O$:B as buffer and transparent conductive oxide layers, Progress in Photovoltaics: Research and Applications, Appl., 28, 79-89 (2020).
3. J. Chantana, Y. Kawano, T. Njshmura, Y. Kimoto, T. Kato, H. Sugimoto, T. Minemoto, Transparent electrode and buffer layer combination for reducing carrier recombination and optical loss realizing over a 22%-efficient Cd-free alkaline-treated Cu(In,Ga)(S,Se)$_2$ solar cell by the all-dry process, ACS Applied Materials and Interfaces, 2, 22298-22307 (2020).
4. S. Sinha, D. K. Nandi, P. S. Pawar, S. H. Kim, J. Heo, A review on atomic layer deposited buffer layers for Cu(In,Ga)Se$_2$ (CIGS) thin film solar cells: Past, present, and future, Solar Energy, 290, 515-537 (2020).
5. W. Witte, D. Hariskos, A. Eicke, R. Menner, O. Kiowski, M. Powalla, Impact of annealing on Cu(In,Ga)Se$_2$ solar cells with Zn(O,S)/(Zn,Mg)O buffers, Thin Solid Films, 535, 180-183 (2013).
6. J. Lindahl, U. Zimmermann, P. Szaniawski, T. Torndahl, A. Hultqvist, P. Salome, C. Platzer-Bjorkman, M. Edoff, Inline Cu(In,Ga)Se$_2$ co-evaporation for high-efficiency solar cells and modules, IEEE J. Photovoltaics, 3, 1100-1105 (2013).
7. K. H. Kim, K. H. Yoon, J. H. Yun, B. T. Ahn, Effects of Se flux on the microstructure of Cu(In,Ga)Se$_2$ thin film deposited by a three-stage co-evaporation process. Electrochem. Solid State Letters, 9, A382-A385 (2006).
8. S. Nishiwaki, T. Satoh, Y. Hashimoto, S. I. Shimakawa, S, Hayashi, T. Negami, T. Wada, Preparation of Zn doped Cu(In,Ga)Se$_2$ thin films by physical vapor deposition for solar cells, Solar Energy Materials and Solar Cells, 77, 359-368 (2003).
9. M. Sugiyama, A. Kinoshita, A. Miyama, H. Nakanishi, S. F. Chichibu, Formation of Zn-doped CuInSe$_2$ films by thermal annealing using dimethylzinc, J. Crystal Growth, 310, 794-797 (2008).
10. C. S. Lee, S. Kim, E. A. Al-Ammar, H. S. Kwon, B. T. Ahn, Effects of Zn diffusion from (Zn,Mg)O buffer to CIGS film on the performance of Cd-free Cu(In,Ga)Se solar cells, ECS J. Solid State Science and Technology, 3, Q99-Q103 (2014).
11. E. Handick, P. Reinhard. J. H. Alsmeier, Leonard Kohler, Fabian Pianezzi, S. Krause, M. Gorgoi, E. Ikenaga, N. Koch, R. G. Wilks, S. Buecheler, A. N. Tiwari, M. Bar, Potassium postdeposition treatment-induced band gap widening at Cu(In,Ga)Se$_2$ surfaces - reason for performance leap?, ACS Applied Materials and Interfaces, 7, 27414-27420 (2015).
12. P. Reinhard, B. Bissig, F. Pianezzi, E. Avancini, H. Hagendorfer, D. Keller, P. Fuchs, M. Dobeli, C. Vigo, P. Crivelli, S. Nishiwaki, S. Buecheler, A. N. Tiwari, Features of KF and NaF postdeposition treatments of Cu(In,Ga)Se$_2$ absorbers for high efficiency thin film solar cells, Chemistry of Materials, 27, 5755-5764 (2015).
13. Y. M. Shin, C. S. Lee, D. H. Shin, H. S. kwon, B. G. Park, B. T. Ahn, Surface modification of CIGS film by annealing and its effect on the band structure and photovoltaic properties of CIGS solar cells, Current Applied Physics. 15, 18-24 (2015).
14. C. H. Ho, Y. C. Chen, Thickness-tunable band gap modulation in γ-In_2Se_3, RSC Advances, 3, 24896-24899 (2013).
15. D. Y. Lyu, T. Y. Chang, S. M. Lan, T. N. Yang, C. C. Chiang, C. L. Chen, H. P. Chiang, Structural and optical characterization of single-phase γ-In_2Se_3 films with room-temperature photo-luminescence, J. Alloys and Compounds, 499,104-107 (2010).
16. D. Y. Lee, J. H. Yun, K. H. Yoon, B. T. Ahn, Characterization of Cu-poor surface on Cu-rich CuInSe$_2$ film prepared by evaporating binary selenide compounds and its effect on solar efficiency, Thin Solid Films, 410, 171-176 (2002).
17. S. C. Kim, Y. M. Ko, S. T. Kim, Y. W. Choi, J. K. Park, B. T. Ahn, Reduction of point defects and Cu surface composition in Cu(In,Ga)Se$_2$ film by Se annealing with a NaF overlayer at intermediate temperatures, Current Applied Physics, 17, 820-828 (2017).
18. S. T. Kim, L. Larina, J. H. Yun, B. Shin, B. T. Ahn, Surface passivation and point defect control in Cu(In,Ga)Se$_2$ films with a Na_2S post deposition treatment for higher than 19% CIGS cell performance, Sustainable Energy Fuels, 3, 709 (2019).
19. S. C. Kim, S. T. Kim, B. T. Ahn, Characterization of atomic-layer

deposited ZnSnO buffer layer for 18%-efficiency Cu(In,Ga)Se_2 solar cells, Current Photovoltaic Research, 3, 54-60 (2015).

20. A. Loubat, S. Béchu, M.Bouttemy, J. Vigneron, D. Lincot, J. Guillemoles, A. Etcheberry, Cu depletion on Cu(In,Ga)Se_2 surfaces investigated by chemical engineering: An x-ray photoelectron spectroscopy approach, Citation: J. Vacuum Science & Technology A, 37, 041201 (2019).
21. C. H. De Groot, J. S. Moodera, Growth and characterization of a novel In_2Se_3 structure, J. Applied Physics, 89, 4336-4340 (2001).
22. J. Weszka, Ph. Danier, A. Burian, A. M. Burian, A. T. Nguyen, Raman scattering in In_2Se_3 and $InSe_2$ amorphous films, J. Non-Crystalline Solids, 265, 98-104 (2000).
23. J. Krustok, H. Collan, K. Hjelt, Does the low-temperature Arrhenius plot of the photoluminescence intensity in CdTe point towards an erroneous activation energy?, J. Applied Physics., 81, 1442-1445 (1997).
24. T. Schmidt, K. Lischka, W. Zulehner, Excitation-power dependence of the near-band-edge photoluminescence of semiconductors, Physical Review B, 45, 8989-8994 (1992).
25. T. Unold and L. Gütay, Photoluminescence Analysis of Thin-Film Solar Cells, Advanced Characterization Techniques for Thin Film Solar Cells, 151-175 (2011).
26. T. Ohtsuka, T. Okamoto, A. Yamada, M. Konagai, Photoluminescence study of γ-In_2Se_3 epitaxial films grown by molecular beam epitaxy, J. Luminescence, 87-89, 293-295 (2000).
27. W. Witte, R. Kniese, M. Powalla, Raman investigations of Cu(In,Ga)Se_2 thin films with various copper contents, Thin Solid Films, 517, 867-869 (2008).
28. R. Caballero, C. A. Kaufmann, V. Efimova, R. Rissom, V. Hoffmann, H. W. Schock, Investigation of Cu(In,Ga)Se_2 thin-film formation during the multi-stage co-evaporation process, Progress in Photovoltaics: Research and Applications, 21, 30-46 (2013).